

**Attenuation of
wave-induced
groundwater pressure
in shallow water.
Part 1**

OCEANOLOGIA, 46 (3), 2004.
pp. 383–404.

© 2004, by Institute of
Oceanology PAS.

KEYWORDS

Surface wave
Pore water pressure
Sandy beach
Filtration

STANISŁAW R. MASSEL
ANNA PRZYBORSKA
MICHAŁ PRZYBORSKI

Institute of Oceanology,
Polish Academy of Sciences,
Powstańców Warszawy 55, PL–81–712 Sopot, Poland;
e-mail: smas@iopan.gda.pl

Manuscript received 31 May 2004, reviewed 28 June 2004, accepted 5 July 2004.

Abstract

A coastal aquifer has a dynamic seaward boundary at the beach face where physical and ecological processes are influenced by oceanic water level fluctuations. Many basic groundwater concepts and the role of the impact of groundwater seepage on beach ecosystems are still poorly understood. Studies are needed to improve our understanding of the relationships between surface and subsurface flow processes on beaches. This is particularly helpful in clarifying the interaction of the physical processes, biodiversity and productivity of sandy beaches, sediment transport and coastal structure stability and modern beach nourishment techniques. As the estimation of infiltration into beach sand is very difficult to carry out under real sea conditions, a control led large-scale laboratory experiment was carried out in the Large Wave Channel in Hannover (Germany) as part of a project supported by the European Community (contract HPRI-CT-2001-00157). First part of the paper describes the technology applied in the experiment and reports some preliminary results.

1. Introduction

The nature of beach groundwater-swash interactions and role of these interactions is of interest to many specialists such as geomorphologists, coastal engineers, sedimentologists, groundwater hydrologists and beach

The complete text of the paper is available at <http://www.iopan.gda.pl/oceanologia/>

ecologists. A coastal aquifer has a dynamic seaward boundary at the beach face, where physical processes are influenced by oceanic water level fluctuations. Most work on beach groundwater behaviour has been done either by coastal engineers, who have tended to oversimplify the hydrological processes, or by hydrologists, who have little knowledge of the implications of the work for swash zone sediment dynamics. However, many basic groundwater concepts, including the impact of groundwater seepage on a beach ecosystem are still poorly understood by coastal researchers. Studies are needed to improve our understanding of the relationships between surface and subsurface flow processes on beaches. They will be particularly helpful in solving the following groups of problems:

- *Interaction of physical processes, biodiversity and productivity of sandy beaches.* Water flow through the beach body is of great importance in introducing water, organic materials and oxygen to the ground environment. Moreover, it controls the vertical and horizontal, chemical and biological gradients, and nutrient exchange in the beach (McLachlan 1989). This provides some basis for assessing the vulnerability of a beach's biodiversity and the functioning of a beach ecosystem, as well as a better understanding of the interaction between tourism, natural changes and the physical marine factors of such an ecosystem (Węśławski et al. 2000).
- *Sediment transport and coastal structure stability.* The water table in beaches lies well above the mean water level because of wave effects. Water table dynamics are of obvious interest in relation to the stability of coastal structures, salt water intrusion to the aquifer, operation of coastal sewage disposal systems and groundwater resource management in coastal areas.
- *Modern beach nourishment techniques.* Beach nourishment to provide an erosion buffer and increase amenity is a well established coastal management option and is favoured because it is a relatively 'soft' option with few aesthetic drawbacks.

As the precise estimation of the extent of run-up, induced infiltration in beach sand, and groundwater table variation are very difficult to carry out under real sea conditions, a controlled large-scale laboratory experiment was performed in the Large Wave Channel (GWK) at the Coastal Research Centre (FZK) in Hannover (Germany). The GWK provides a unique opportunity for such an experiment. The simulation of regular and random waves with prescribed spectra yields a very realistic pattern of the sea

surface. Moreover, the excellent testing facilities help substantially in recording the extent of run-up on the beach face, its velocity, and the amount of water infiltrating into the beach body.

The project was funded by the European Community within the Access to Research Infrastructures Action of the Human Potential Programme (contract HPRI-CT-2001-00157). The aim of this paper is to describe the technology used in the experiment and to report some preliminary results. A more comprehensive analysis of wave-induced pressure and groundwater circulation is now in preparation as a Part 2 of the paper.

This paper is organised as follows. The scientific background of the project is presented in Section 2. Section 3 contains a description of the basic facilities of the Large Wave Channel. In Section 4, preliminary results of the experiment are presented and some comparisons with theoretical formulas are given. In particular, two different pore pressure components are distinguished and the mechanisms of their generation are discussed. Finally, Section 5 contains conclusions and proposals for further studies.

Additionally, to take full advantage of our access to the GWK facilities, two other experiments were carried out. The first experiment was dedicated to the relationships between underwater noise and the intensity of wave breaking in deep water as well as on the beach. The results of this experiment will be presented in an other paper, now in preparation (Klusek & Lisinienka, to be published). The second experiment examined the dynamics of ripple formation with slowly changing water depth.

2. Scientific background of the project

For tideless seas the groundwater flow is governed entirely by the surface wave dynamics on the beach. As waves propagate towards the shore, they become steeper owing to the decreasing water depth and at some depth, the waves lose their stability and start to break. When waves break, wave energy is dissipated and the spatial changes of the radiation stress give rise to changes in the mean sea level (MSL), known as the set-up. Longuet-Higgins (1983) demonstrated that the mean on-shore pressure gradient due to wave set-up drives a groundwater circulation within the beach zone. Water infiltrates into the coastal aquifer on the upper part of the beach near the maximum run-up, and exfiltration occurs on the lower part of the beach face near the breaking point.

After the wave reaches the shore, it will run up and run down the beach face. A number of papers in recent years (Nielsen 1990, Aseervatham et al. 1993, Kang et al. 1994, Kang & Nielsen 1996, Li et al. 1997, Li & Barry 2000) have reported on the results of field, laboratory and theoretical studies of wave set-up and water table fluctuations. The experiments isolating

tidal effects showed reasonable agreement with an analytical solution of the Boussinesq equation for a sloping beach with a large tidal amplitude. In the case of short waves, mathematical models of the water table that includes the effects of wave run-up infiltration were developed in a steady state. Saturated flow was considered in most of the solutions. Recently, however the existence of a capillary fringe above the beach water table has been confirmed by field measurements. Capillary effects provide a mechanism for high-frequency water table fluctuations in the aquifer. These fluctuations are standing wave-like with the amplitude becoming increasingly damped inland (Li et al. 1997).

It should be noted that two types of pore pressure can be distinguished in the observed experimental data. In the zone of non-breaking waves, only the so-called phase-resolving type of pore pressure exists when the pore pressure responds almost instantaneously to surface wave oscillations. On the other hand, two types of pore pressure are generated in the surf zone. Apart from the phase-resolving pore pressure component, a slowly varying pore pressure component is observed. This component is called the phase-averaged pressure when the pressure slowly increases from the initial zero value to some asymptotic value as a result of wave action. The value of the phase-averaged pressure depends on the gradient of the excess static pressure induced at the sea bottom due to the wave set-up in the surf zone.

In the laboratory experiments reported in this paper both types of pressure were recorded and their nature will be discussed in the following sections.

3. Basic facilities in the Large Wave Channel

As was mentioned in Section 2, despite improvements in modelling technology, many basic groundwater concepts are still poorly understood. In particular, the relationship between wave run-up, infiltration velocity, and water table fluctuation in unsaturated flow requires further analysis. Furthermore the infiltration due to irregular wave run-up and its connection with the run-up are not well known. The reported laboratory experiments have been done in relatively small scales and the scale effects of such experiments are difficult to estimate. On the other hand, field experiments have frequently been inconclusive owing to side effects. These facts demonstrate the necessity for controlled laboratory experiments in an almost natural scale.

The experiments reported here were carried out in the largest channel in Europe – the Large Wave Channel (GWK – Grosser Wellenkanal) in Hannover (Germany). The channel is 307 m long, 5 m wide and 7 m deep

(see Fig. 1). The installed power of the piston type wave generator combined with an upper flap is about 900 kW. The gearwheel driven carrier gives a maximum stroke of ± 2.10 m to the wave paddle. The stroke can be superimposed by an upper flap oscillating within ± 10 degrees in order to simulate shorter wave kinematics more accurately. As a result, waves (regular or irregular) up to a height of 2.00 m can be simulated.



Fig. 1. Large Wave Channel in Hannover

Wave generation is controlled by an online absorption system. This special system works with all kinds of regular and irregular wave trains. Thus, the tests are unaffected by re-reflections at the wave generator and can be carried out for a nearly unlimited duration. The wavemaker also allows the generation of freak waves breaking at a predetermined point of the channel.

During the experiment, a water depth of 4 m in front of the beach was assumed. Natural beach sand with the main characteristics given in Table 1 and in Figs 2 and 3 was used and a uniform beach with a 1:20 slope was created in the channel. To measure the pore water pressure, four systems of pressure gauges were installed along the beach face (see Fig. 4). In each system, four piezoelectric pressure sensors were fixed to a metal rod arranged in the form of a cross (Fig. 5a). Such an arrangement provides an opportunity to estimate not only the pore pressure, but also the horizontal and vertical water velocities in the beach body. Initially, the sensors in all

Table 1. Sand sample characteristics (sampling date: 02.10.2003; sampling place: GWK, Hannover)

Grain size [mm]	Fraction weight [g]	Share of fraction	Cumulative share [%]
2.0	0.0	0.0	0.0
1.0	1.15	0.075	0.075
0.5	4.93	2.465	2.54
0.25	93.78 (+1.61)	47.695	50.235
0.125	93.19	46.595	96.83
0.063	6.16	3.08	99.91
Bottom	0.18	0.09	100.00
Total	198.39	100.00	Analytical error: 0.805%

Granulometric analyses: sieve analyses; done by K. Czerniak
Sample weights [g]: 200.00; date of analyses: 21.10.2003

Mean diameter (1st moment) = 2.51 – fine grained sand
Standard deviation (2nd moment) = 0.63 – moderately well sorted sand
Skewness (3rd moment) = 0.59 – insignificant diagonal positive curve
Kurtosis (4th moment) = 7.61 – moderately steep curve

Organic matter content: 0.222%
Porosity: 26%
Very fine fraction content: 0.0708% (0.0354 g) containing a:
Very fine organic fraction: 0.0112% (0.0056 g)
Very fine inorganic fraction: 0.0596% (0.0298 g)

Macroscopic description: fine-grained sand, well sorted, moist, colour:
yellow-grey, flora/ fauna – none, admixtures – none, HCl – no reaction

the systems were installed as shown in Fig. 5b. However, due to sediment motion induced by the wave action, the profile of the sandy bottom was changed in some tests.

The pore pressure System 1 was located at the waterline, while Systems 3 and 2 were in the run-up and run-down zone, respectively. Additionally, System 4 was placed in front of the breaking zone, where set-up due to radiation stress was not observed (see Fig. 4).

In the experiment, twenty one wave gauges were distributed along the channel in the deep-water zone, surf zone and run-up zone. The location of the wave gauges in the surf and run-up zones is shown in Fig. 6.

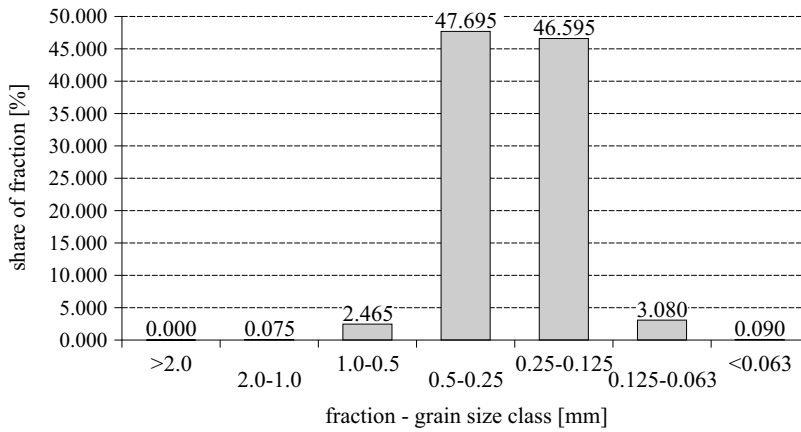


Fig. 2. Grain size distribution

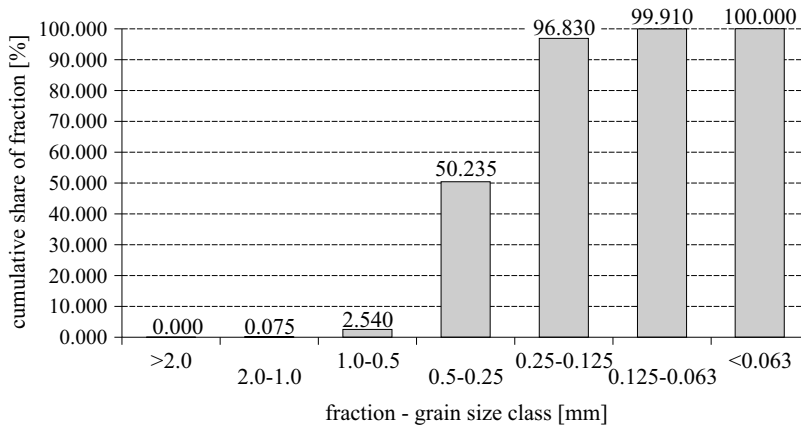


Fig. 3. Cumulative grain size distribution

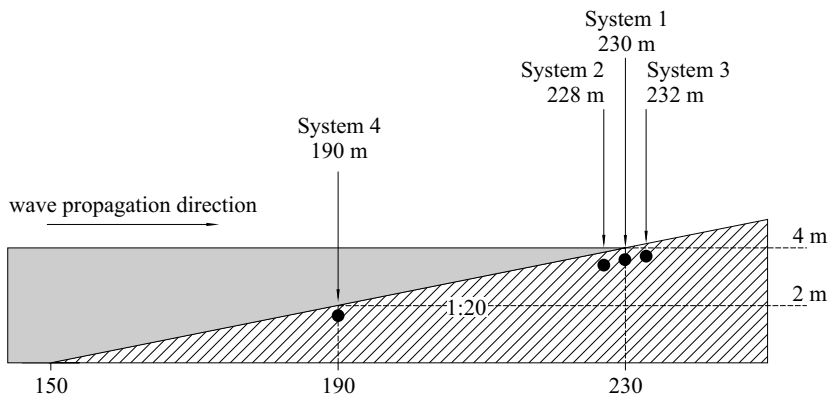


Fig. 4. Location of the pore pressure gauges on the sandy beach



Fig. 5a. Pore pressure gauge system

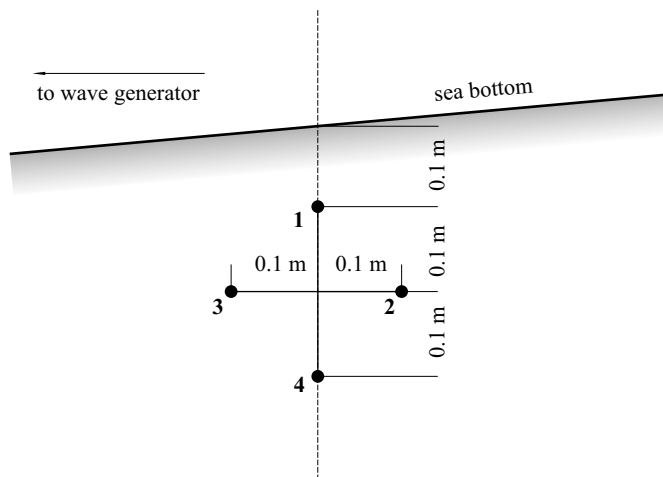


Fig. 5b. Submergence of pore pressure gauges in the beach sand

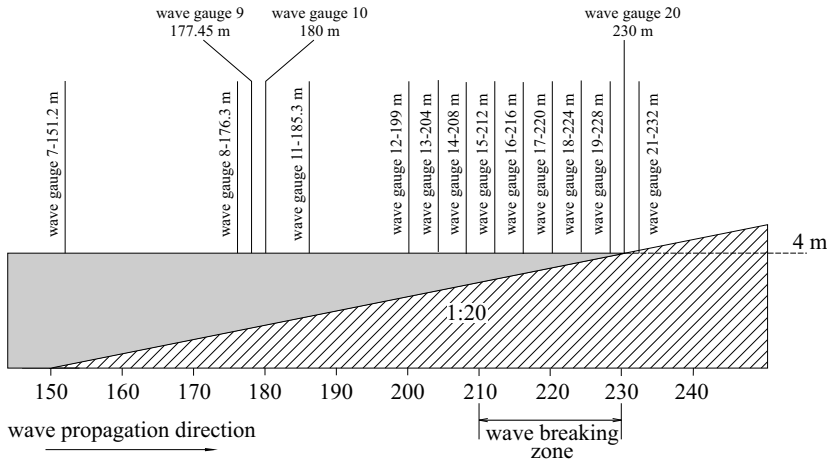


Fig. 6. Location of wave gauges at distances between 150 m and 240 m from the wave generator

4. Preliminary results of the experiment

4.1. Scope of the experiment

A total of 55 tests were carried out in the experiment and all wave and pore water pressure data were saved in a prescribed format. Regular waves were used in 42 tests, and irregular waves, with the JONSWAP spectrum, were used in 13 tests. In each test about 200 waves were generated, with some additional time for wave onset and then for wave return to rest.

The characteristics of all the tests with regular waves are summarized in Table 2. In particular, X_{br} denotes the distance of the wave breaking point

Table 2. Experiments with regular waves

Number of test	File (number)	Wave height H [m]	Wave period T [s]	Water depth h [m]	X_{br} [m]	X_{min} [m]	X_{max} [m]
1	20110301	0.4	8.0	4.00	219.0	233.0	237.0
2	20110302	0.5	8.0	4.00	215.5	230.0	237.5
3	20110303	0.6	6.0	4.00	215.5	230.0	237.8
4	21110301	0.4	10.0	4.00	216.5	233.5	238.0
5	21110302	0.4	5.0	4.00	219.0	231.0	234.2
6	21110303	0.3	6.0	4.00	220.0	230.0	234.0
7	21110304	0.3	10.0	4.00	219.0	230.0	236.5
8	24110301	0.2	8.0	4.00	223.5	229.0	235.0

Table 2. (*continued*)

Number of test	File (number)	Wave height H [m]	Wave period T [s]	Water depth h [m]	X_{br} [m]	X_{min} [m]	X_{max} [m]
9	24110302	0.4	6.0	4.00	219.0	232.0	236.0
10	24110303	0.3	5.0	4.00	221.0	229.0	233.0
11	24110304	0.3	7.0	4.00	221.5	228.0	236.0
12	24110305	0.6	8.0	4.15*	218.0	236.0	241.0
13	24110306	0.2	9.0	4.00	224.0	230.0	235.0
14	24110307	0.5	6.0	4.00	218.0	230.0	234.0
15	24110308	0.4	7.0	4.00	219.0	229.5	233.0
16	24110309	0.3	9.0	4.00	219.0	228.0	234.0
17	25110301	0.2	7.0	4.00	223.5	229.0	233.0
18	25110302	0.6	5.0	4.00	216.5	229.5	234.5
19	25110303	0.8	6.0	4.00	213.5	230.0	235.5
20	25110304	0.5	7.0	4.00	215.0	229.5	234.0
21	25110305	0.6	9.0	4.00	214.0	228.5	240.0
22	25110306	0.2	6.0	4.00	224.0	229.5	232.0
23	25110307	0.5	5.0	4.00	214.0	229.5	233.5
24	25110308	0.6	7.0	4.00	214.5	229.0	235.0
25	26110301	0.7	5.0	4.00	214.5	230.0	234.0
26	26110302	0.8	5.0	4.00	214.0	230.5	235.0
27	26110303	0.7	6.0	4.00	214.0	229.5	236.0
28	26110304	0.7	7.0	4.00	214.0	228.0	240.0
29	26110305	0.8	7.0	4.00	212.0	230.0	238.0
30	26110306	0.8	8.0	4.00	212.0	230.0	240.0
31	26110307	0.3	8.0	4.00	220.0	229.0	234.0
32	26110308	0.7	8.0	4.00	212.0	229.0	237.5
33	27110301	0.8	9.0	4.00	212.0	230.0	240.5
34	27110302	0.7	9.0	4.00	212.5	230.0	240.0
35	27110303	0.8	10.0	4.00	212.0	230.0	241.5
36	27110304	0.7	10.0	4.00	212.0	229.5	241.0
37	27110305	0.5	10.0	4.00	213.5	229.0	237.5
38	27110306	0.5	9.0	4.00	214.0	227.5	236.5
39	27110307	0.6	10.0	4.00	212.5	227.0	241.0
40	27110308	0.2	10.0	4.11*	226.0	228.0	236.0
41	28110301	0.4	9.0	4.11*	224.0	229.0	233.0
42	28110302	0.2	5.0	4.10*	224.0	229.0	233.0

* water depth other than 4.00 m.

from the wave generator, X_{\min} is the location of the maximum wave run-down on the beach and X_{\max} is the location of the maximum wave run-up on the beach.

Table 3 contains the wave characteristics of tests with irregular waves. As far as the irregular waves are concerned the wave breaking point changed substantially; only the minimum distance of the wave breaking point X_{br} and the distance of maximum wave run-up X_{\max} on beach are given.

Table 3. Experiments with irregular waves

Number of test	File (number)	H_s [m]	T_p [s]	Water depth h [m]	H_{\max} [m]	X_{br} [m]	X_{\max} [m]
43	28110303	0.2	6.0	4.10	0.330	221.0	235.0
44	01120301	0.4	6.0	4.10	0.660	214.0	–
45	02120301	0.6	6.0	4.10	0.784	212.0	244.0
46	02120302	0.8	6.0	4.10	1.046	206.0	248.0
47	02120303	0.2	7.0	4.10	0.261	224.0	236.0
48	02120304	0.4	7.0	4.10	0.523	216.0	240.0
49	02120305	0.6	7.0	4.10	0.784	214.0	242.0
50	02120306	0.8	7.0	4.10	1.046	204.0	248.0
51	02120307	1.0	7.0	4.10	1.731	196.0	251.0
52	03120301	1.0	6.0	4.10	1.731	192.0	250.0
53	03120302	0.2	8.0	4.10	0.261	223.0	238.0
54	03120303	0.4	8.0	4.08*	0.692	212.0	241.0
55	03120304	0.6	8.0	4.08*	0.784	212.0	244.0

* water depth other than 4.00 m; symbols: H_s – significant wave height, T_p – peak wave period.

4.2. Phase-resolving pressure component

In order to illustrate the phase-resolving pressure component in Fig. 7, the results of Test 25 for System 4, located at a distance of 190 m from the wavemaker, are shown. The water surface oscillations are given in the upper part of the figure. However, these oscillations do not correspond exactly to the location of the pressure gauge, as they correspond to the nearest wave gauge located at distance $X = 185.30$ m.

The water depth in System 4 was $h = 2.0$ m. Pore pressure gauge 41 is located 10 cm below the sea bottom, while gauges 42 and 43 are 20 cm, and gauge 4 – 30 cm below the sea bottom. The figure indicates that the oscillations of surface waves as well as these of the corresponding pore pressure at these three levels are relatively stable. As System 4 is located in

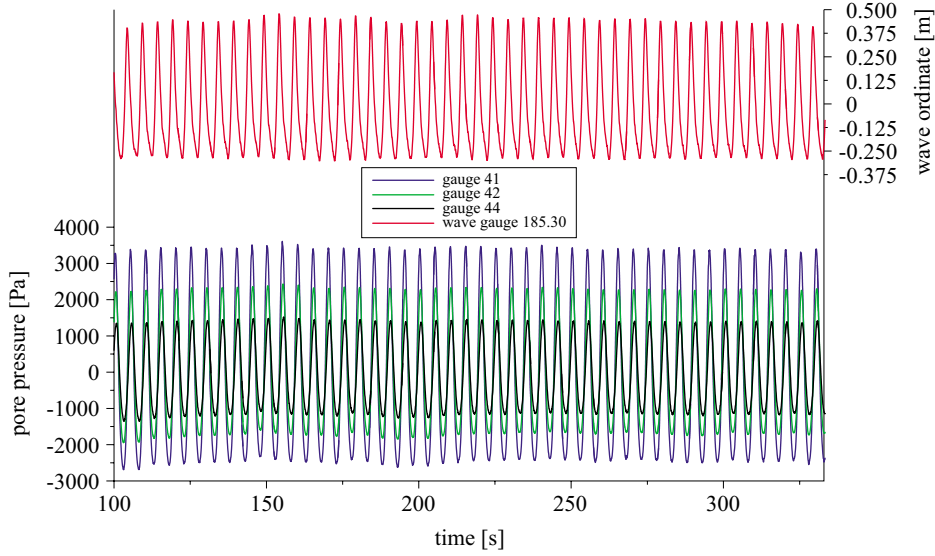


Fig. 7. Wave surface and pore pressure oscillations in System 4 ($x = 190$ m) for Test 25 ($H = 0.7$ m, $T = 5.0$ s)

front of the breaking zone, the observed pore pressure belongs entirely to the phase-resolving pressure component, where the pore pressure corresponds directly to the oscillations of the sea surface. However, the mean value of the pore pressure remains zero.

A simple linear wave model indicates that the amplitude of water pressure at the sea bottom (in our case $z = h = -2.0$ m) is given by (Massel 2001):

$$p_0 = p(x_0, z = -h) = \frac{\rho_w g A(x_0)}{\cosh(kh)}, \quad (1)$$

in which $\rho_w = 1000 \text{ kg m}^{-3}$ is the water density, ω is the wave frequency, $A(x_0)$ is the wave amplitude in the vicinity of System 4 and k is the wave number satisfying the classical dispersion relation

$$\omega^2 = \left(\frac{2\pi}{T}\right)^2 = gk \tanh(kh). \quad (2)$$

The pore pressure p_0 induced by surface waves attenuates in a porous beach with distance from the sea bottom. In Fig. 8, the normalised pore pressure p/p_0 is shown as a function of the total pressure gauge submergence. In all, 28 test results were used in the figure. The corresponding Ursell number $U = \frac{H}{h} \left(\frac{L}{h}\right)^2$, indicating the level of wave nonlinearity, is in the range of 18–134 (Massel 1989).

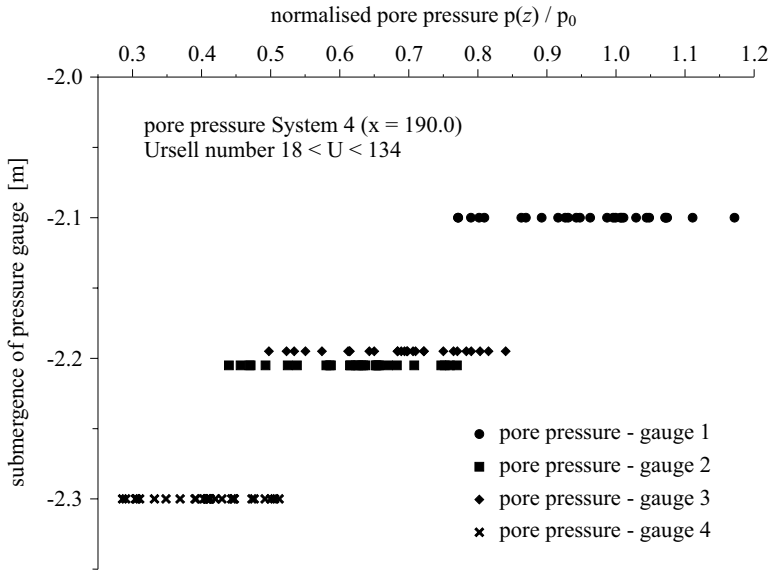


Fig. 8. Normalised pore pressures $p(z)/p_0$ in System 4 ($x = 190$ m) for all 28 tests

The figure indicates that pore pressure attenuates strongly with submergence. However, the scattering of experimental points at each level of submergence is relatively large. Such a result indicates that attenuation of the normalised pore pressure is much more complicated and does not depend on the function of submergence z and a Ursell number only.

From the theory of multi-phase media, described in Part 2 of the paper, it can be shown, that attenuation of the phase-resolving pore pressure is given by the function

$$p_{pr}(z) = \rho_w g A \frac{\cosh[\psi(z + h_n)]}{\cosh(kh) \cosh[\psi(h_n - h)]} \exp[i(kx - \omega t)]$$

for $-h_n \leq z \leq h$ (3)

or

$$p_{pr}(z) = p_0 \left| \frac{\cosh[\psi(z + h_n)]}{\cosh[\psi(h_n - h)]} \right| \cos(kx - \omega t + \varphi),$$
 (4)

in which φ is the phase lag between the surface oscillation and pore pressure at given z , h_n is the depth of a non-porous bottom and $(h_n - h)$ is the thickness of the porous layer. The wave number ψ is a complex quantity such as

$$\psi = |\psi| \exp(i\theta),$$
 (5)

in which

$$|\psi| = k \left\{ 1 + \frac{\omega^2(\rho_w g)^2}{k^4 K_f^2} \left[\frac{n}{E'_w} + \frac{1}{G} \frac{1-2\nu}{2(1-\nu)} \right]^2 \right\}^{1/4} \quad (6)$$

and

$$\theta = \frac{1}{2} \arctan \left\{ -\frac{\omega(\rho_w g)^2}{k^2 K_f} \left[\frac{n}{E'_w} + \frac{1}{G} \frac{1-2\nu}{2(1-\nu)} \right] \right\}, \quad (7)$$

where n is the porosity of the sand, K_f [m s⁻¹] is the coefficient of permeability,

$$G = \frac{E_s}{2(1+\nu)} \quad (8)$$

is the shear modulus of the solid matrix, E_s is the bulk modulus of the solid matrix, ν is the Poisson coefficient, and E'_w is the bulk modulus of the pore water. E'_w depends on the air content according to the formula

$$\frac{1}{E'_w} = \frac{1}{E_w} + \frac{1-S}{p_0}, \quad 1-S \ll 1, \quad (9)$$

in which $E_w = 2.3 \times 10^9$ N m⁻² is the bulk modulus of water without air and S is the degree of saturation.

Therefore, the normalised amplitude of the phase-resolving pore pressure takes the form

$$\frac{|p_{pr}(z)|}{p_0} = \left| \frac{\cosh[\psi(z+h_n)]}{\cosh[\psi(h_n-h)]} \right|. \quad (10)$$

If we neglect the compressibility of water and the shear modulus of the solid matrix in eq. (3), we obtain

$$\frac{|p_{pr}(z)|}{p_0} = \frac{\cosh[k(z+h_n)]}{\cosh[k(h_n-h)]}, \quad (11)$$

which corresponds to the potential solution representing Darcy's flow (Massel 2001).

In Figs 9–13, the attenuation of the phase-resolving pressure with the submergence of the pressure gauges is shown for four tests (tests 10, 23, 3, 7, 4) with different Ursell numbers. The experimental data on pore pressure at four pressure gauges are supplemented by the attenuation resulting from eqs. (10) and (11). For the bottom material – fine grained sand – the bulk modulus of the solid matrix $E_s = 10^8$ N m⁻² and the coefficient of permeability $K_f = 8 \times 10^{-4}$ m s⁻¹ were adopted. The unknown bulk modulus of pore water E'_w was selected to give the best fit of the experimental data. The figures indicate

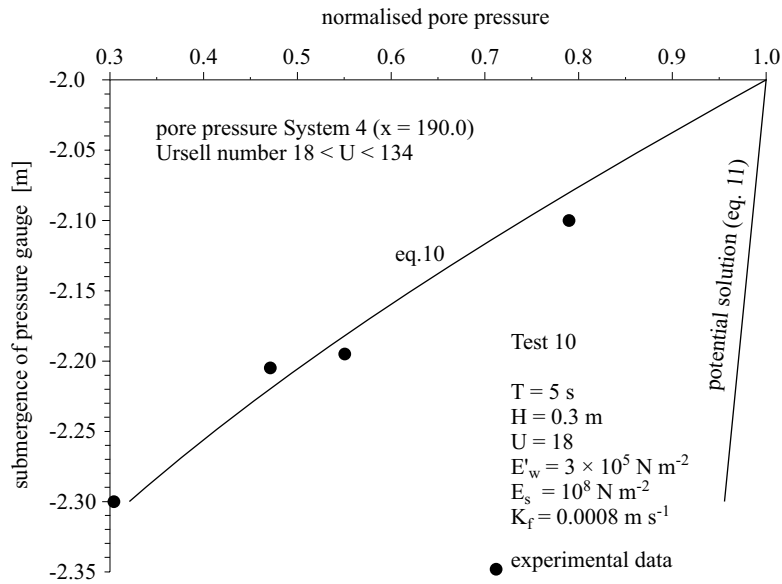


Fig. 9. Attenuation of normalised phase-resolving pressure with submergence of pressure gauges for Ursell number $U = 18$

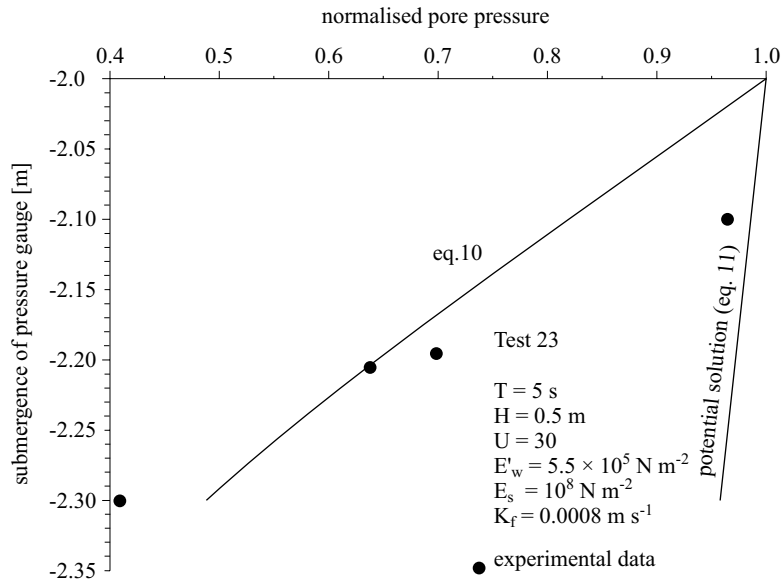


Fig. 10. Attenuation of normalised phase-resolving pressure with submergence of pressure gauges for Ursell number $U = 30$

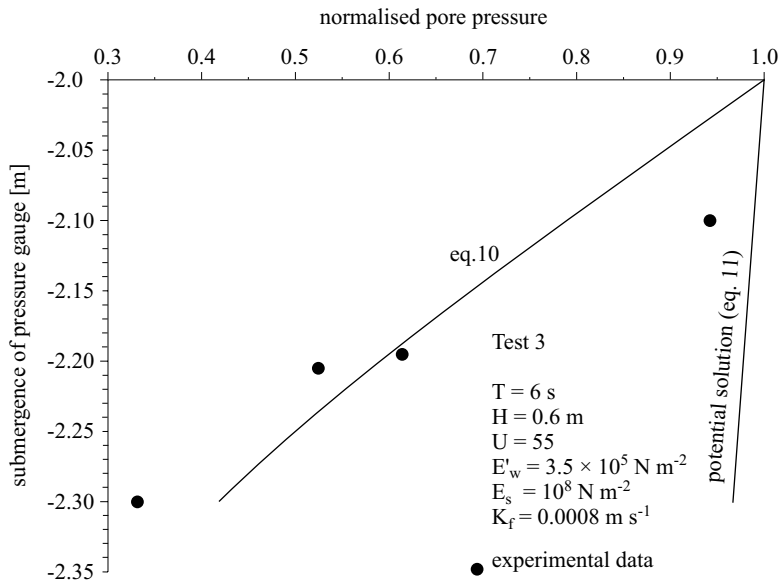


Fig. 11. Attenuation of normalised phase-resolving pressure with submergence of pressure gauges for Ursell number $U = 55$

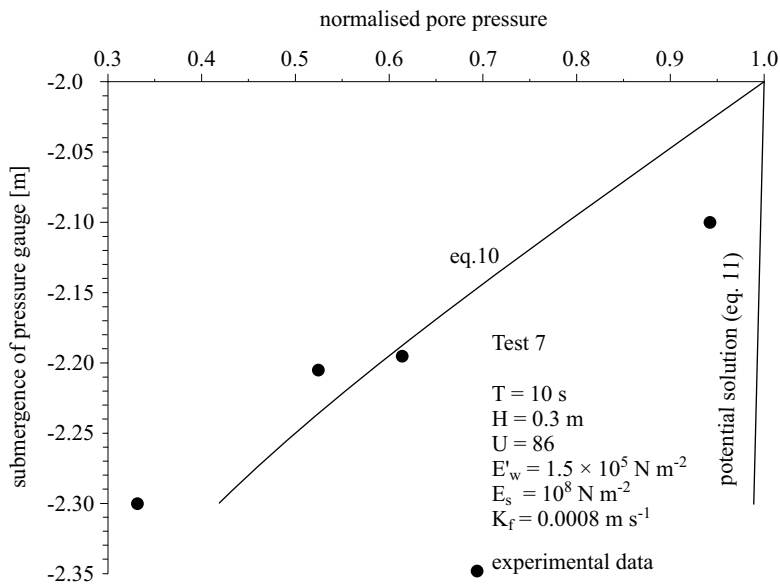


Fig. 12. Attenuation of normalised phase-resolving pressure with submergence of pressure gauges for Ursell number $U = 86$

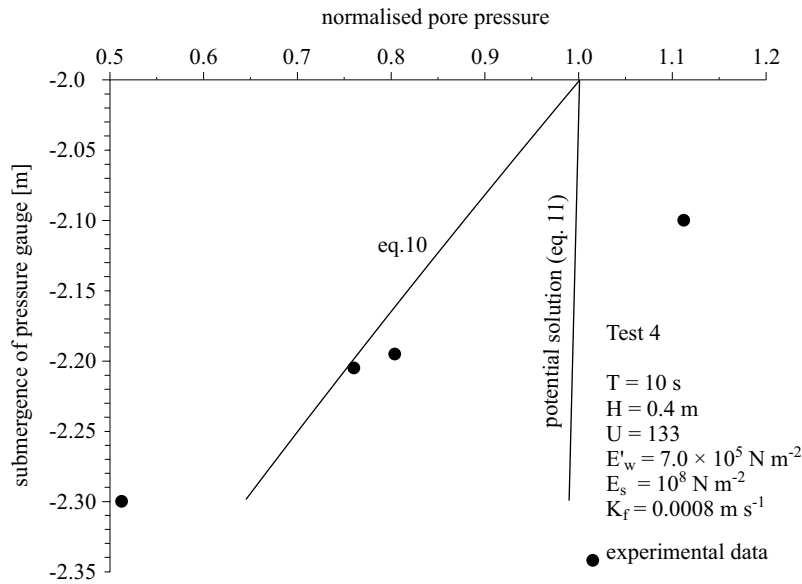


Fig. 13. Attenuation of normalised phase-resolving pressure with submergence of pressure gauges for Ursell number $U = 133$

that E'_w is in the range of $1.5 \times 10^5 \text{ N m}^{-2} - 7 \times 10^5 \text{ N m}^{-2}$, which means that the degree of saturation is rather low, and the air content is high, depending on the dynamics of the surface waves. It should be noted that the attenuation of pore pressure according to eq. (11) is very small and does not correspond to the observed values. Therefore, the attenuation of pore pressure in the experiment cannot be modelled by the simple Darcy's law.

4.3. Phase-averaged pressure component

Fig. 14 shows the pore pressure recorded at three gauges during Test 25 at $X = 230 \text{ m}$ (System 1 – intersection of sea bottom and water level). Two components of the pore pressure are clearly seen. In particular, at time $T > 250$ seconds, the non-zero phase-averaged component is almost constant.

As was mentioned above, the mean water level in the surf zone changes as a result of the radiation stress mechanism (set-up). Additional static pressure is therefore created at the sea bottom. The non-zero spatial gradient of this pressure induces an excess pore pressure and generates a pore-water circulation in the beach body (Massel 2001). Fig. 15 illustrates the set-up calculated for the wave parameters used in Test 25 ($H = 0.7 \text{ m}$, $T = 5 \text{ s}$). The method of calculating the set-up is explained in other papers, for example, Massel & Brinkman (2001).

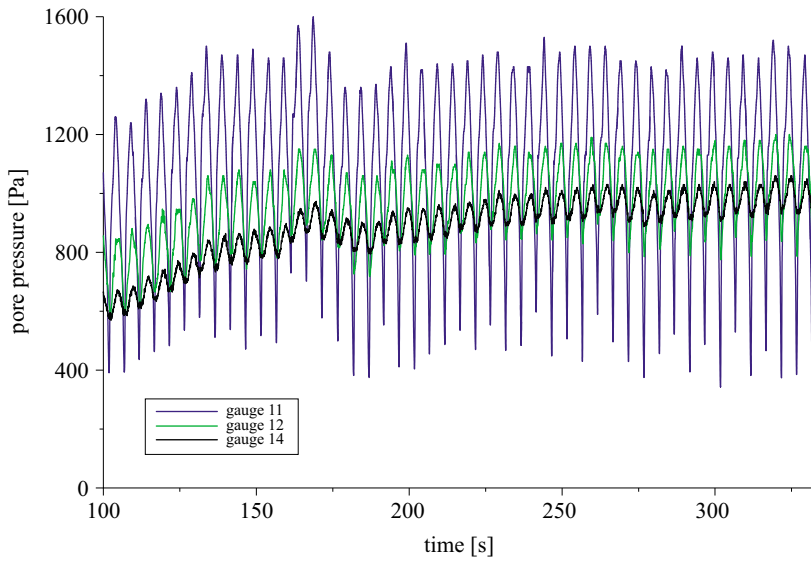


Fig. 14. Pore pressure oscillation in System 4 ($x = 23$ m) for Test 25 ($H = 0.7$ m, $T = 5.0$ s)

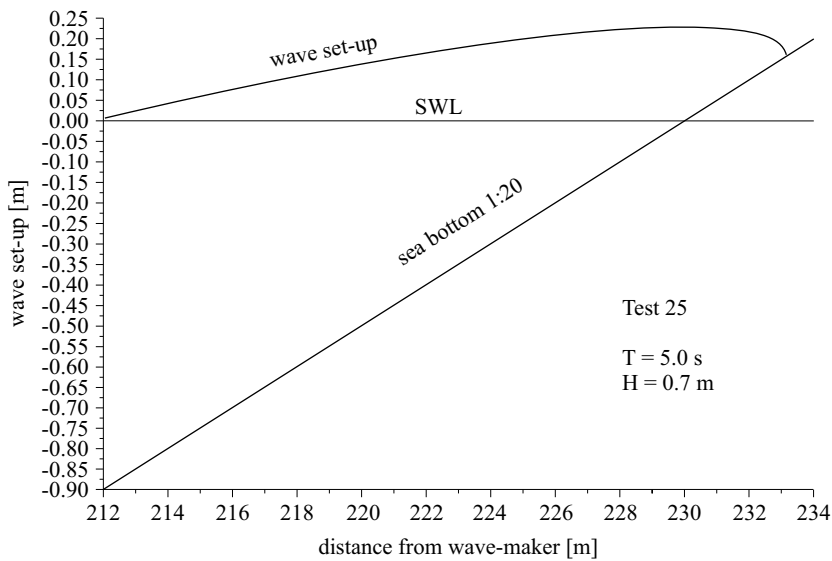


Fig. 15. Wave set-up for Test 25 ($H = 0.7$ m, $T = 5.0$ s)

The maximum set-up at $X = 230$ m is equal to $\bar{\zeta}_{\max} = 0.228$ m. This corresponds to a maximum static excess pressure of $p_{st}^{(\max)} = \rho g \bar{\zeta}_{\max} = 2236$ Pa induced at the sea bottom. From Fig. 14 it follows that pressure $p_{st}^{(\max)}$

generates a phase-averaged pressure of about 965 Pa at gauge 11, 1056 Pa at gauge 12, 1069 Pa at gauge 13 and 1067 Pa at gauge 14. On the other hand, the amplitudes of the phase-resolving pressures are: gauge 11–507 Pa, gauge 12–175 Pa, gauge 13–131 Pa and gauge 14–61 Pa. It should be noted that because of slight erosion, the submergence of the gauges in the sand was slightly changed from its initial position. For gauge 11 it was 0.08 m, while for gauges 12 and 13 it was 0.18 m, and for gauge 14 it was 0.28 m.

The total pressure recorded by the pressure gauge is simply a summation of the phase-averaged and phase-resolving components:

$$p(x_0, z, t) = p_{pa}(x_0, z) + p_{pr}(x_0, z, t). \tag{12}$$

It should be noted that an attempt to model the attenuation of the phase-averaged pressure and induced water circulation was made in another paper (Massel 2001).

4.4. Kinematics of the underwater flow

Owing to spatial pore pressure gradients the pore water circulates within the beach body. In the experiment we were not able to measure the flow velocity in a straightforward manner. However, the flow velocity can be estimated from the pressure measurements using the formulas resulting from the potential solution (Massel 2001):

$$\left. \begin{aligned} u &= -\frac{K_f}{\rho_w g} \frac{\partial p}{\partial x} \\ w &= -\frac{K_f}{\rho_w g} \frac{\partial p}{\partial z} \end{aligned} \right\}. \tag{13}$$

Using simultaneous pore pressure records at the four gauges we can approximate the nondimensional velocity components \tilde{u} and \tilde{w} from eqs. (13) as follows:

$$\tilde{u} = \frac{u}{K_f} = -\frac{1}{\rho_w g} \frac{p(x_2, z_2, t) - p(x_3, z_3, t)}{2\Delta x}, \tag{14}$$

$$\tilde{w} = \frac{w}{K_f} = -\frac{1}{\rho_w g} \frac{p(x_1, z_1, t) - p(x_4, z_4, t)}{2\Delta z}, \tag{15}$$

in which $\Delta x = \Delta x = 0.1$ m, $x_1 = x_4 = 230.0$ m, $x_2 = 229.9$ m, $x_3 = 230.1$ m, $z_1 = -2.08$ m, $z_2 = z_3 = -2.18$ m and $z_4 = -2.28$ m.

By way of illustration, the pore pressures at the four gauges of System 1 and the nondimensional velocity components \tilde{u} and \tilde{w} for Test 25 are shown in Fig. 16. The upper part of the figure confirms clearly the superposition of the phase-averaged and phase-resolving pressures. As expected, the pore pressure exhibits a periodic character with a wave period of $T = 5$ s. Simultaneously, the pressure attenuates with the submergence of the gauge into the porous medium. At gauges 12 and 13, the records are very similar

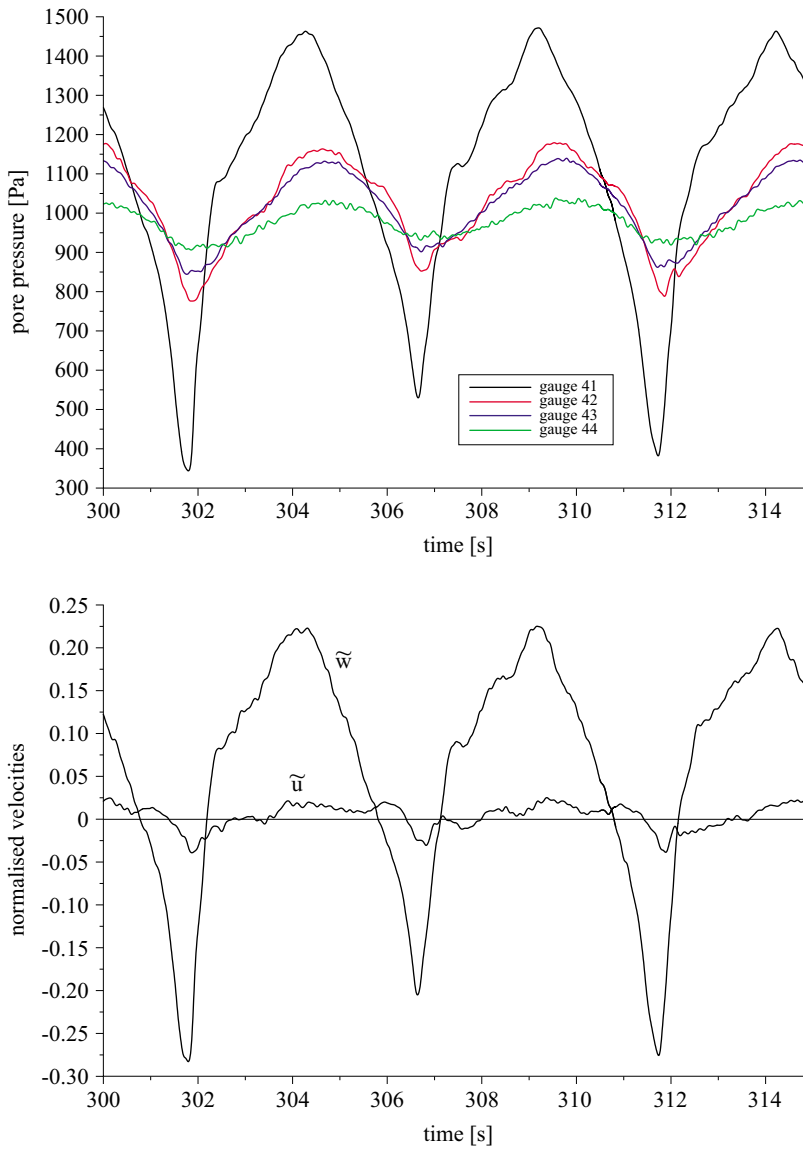


Fig. 16. Pore pressure and pore water velocity oscillations in System 4 ($x = 230$ m) for Test 25 ($H = 0.7$ m, $T = 5.0$ s)

as these gauges are located at the same submergence (c. 18 cm). A small phase lag between those records is due to the horizontal shift (~ 20 cm) of gauge 13 with respect to gauge 12.

The normalised velocity components, shown in the lower part of Fig. 16, are also quasiperiodic. However, the vertical velocity component is much greater than the horizontal one. This means that at point 1 ($x = 230$),

located at the intersection of the still water level with the sea bottom, the pore water is moving in an almost vertical direction. If we assume that $K_f = 0.0008 \text{ m s}^{-1}$ for fine grained sand, the maximum pore water velocity for Test 25 is of the order of 0.2 mm s^{-1} .

Conclusion and further studies

The tests carried out at the Coastal Research Centre provide a substantial amount of very unique experimental data on surface-wave-induced pore pressure. In particular, under controlled and almost full-scale conditions, the dual nature of the pore pressure has been detected. It was found that beyond the breaker zone, only the so-called phase-resolving pressure is observed, while within the surf zone, the phase-resolving component as well as the phase-averaged pressure component are recorded. The pore pressure gradients provide valuable information on the kinematics of groundwater flow in the beach body. The data collected will be used for comparison with the theoretical results which are now in preparation.

Acknowledgements

The large scale tests at the LARGE WAVE CHANNEL (GWK) of the Coastal Research Centre (FZK) were supported by the European Community under the Access to Research Infrastructures Action of the Human Potential Programme (contract HPRI-CT-2001-00157).

Dipl. Eng. J. Grüne from the Coastal Research Centre (FZK) and his staff, as well as Mr. J. Dąbrowski, Mr. K. Waśkowicz and M. Eng. M. Wichorowski from the Institute of Oceanology are gratefully acknowledged for their very helpful assistance with the experimental observations.

References

- Aseervatham A. M., Kang H. Y., Nielsen P., 1993, *Groundwater movement in beach watertables*, 11th Austr. Coastal and Ocean Eng. Conf., 1, 589–594.
- Kang H. Y., Nielsen P., 1996, *Watertable dynamics in coastal areas*, Proc. 26th Conf. Coastal Eng., 3, 4601–4612.
- Kang H. Y., Nielsen P., Hanslow D. J., 1994, *Watertable overheight due to wave run-up on a sandy beach*, Proc. 25th Conf. Coastal Eng., 2, 2115–2124.
- Klusek Z., Lisinienka A., *Acoustics of breaking waves*, (to be published).
- Li L., Barry D. A., 2000, *Wave-induced beach groundwater flow*, Adv. Water Resour., 23, 325–337.
- Li L., Barry D. A., Parlange J.-Y., Pattiaratchi C. B., 1997, *Beach water table fluctuations due to wave run-up: Capillary effects*, Water Resour. Res., 33, 935–945.

- Longuet-Higgins M. S., 1983, *Wave set-up, percolation and undertow in the surf zone*, Proc. R. Soc. Lond., A390, 283–291.
- Massel S. R., 1989, *Hydrodynamics of coastal zones*, Elsevier, Amsterdam, 336 pp.
- Massel S. R., 2001, *Circulation of groundwater due to wave set-up on a permeable beach*, Oceanologia, 43 (3), 279–290.
- Massel S. R., Brinkman R. M., 2001, *Wave-induced set-up and flow over shoals and coral reefs. Part 1. A simplified bottom geometry case*, Oceanologia, 43 (4), 373–388.
- McLachlan A., 1989, *Water filtration by dissipative beaches*, Limnol. Oceanogr., 34, 774–780.
- Nielsen P., 1990, *Tidal dynamics of the water table in beaches*, Water Resour. Res., 26, 2127–2134.
- Węsławski J. M., Urban-Malinga B., Kotwicki L., Opaliński K., Szymelfening M., Dutkowski M., 2000, *Sandy coastlines – are there conflicts between recreation and natural values?*, Oceanol. Stud., 29 (2), 5–18.